Check for updates

CELL BIOLOGY

Transcriptional control of meiotic recombination by DREAM complex components

Hasibe Tunçay[1,2], Xing Ma[3], Katja Müller[1], Yuxuan Guo[4], Valerio Filippo Toccaceli[1], Huiqi Fu[1], Franziska Böwer[1], Lucas Lang[1]†, David Latrasse[3], Yingxiang Wang[5], Moussa Benhamed[3], Arp Schnittger[1]*

Copyright © 2026 The Authors, some rights reserved; exclusive licensee American Association for the Advancement of Science. No claim to original U.S. Government Works. Distributed under a Creative Commons Attribution NonCommercial License 4.0 (CC BY-NC).

Meiotic chromosome segregation and recombination, essential for sexual reproduction and evolution, require a specialized gene set. Despite its importance, the transcriptional regulators that directly orchestrate meiotic gene expression remain unidentified in plants. We identify the MuvB core components known from the DREAM complex as key transcriptional regulators of meiotic recombination in *Arabidopsis*. Loss of DREAM components TCX5/6 and ALY1/2 leads to impaired recombination and fertility defects. Meiocyte-specific transcriptome profiling and genome-wide binding analyses reveal that core recombination genes, including the crossover-promoting helicase MER3, are direct targets. Consistently, *MER3* overexpression partially rescues recombination defects in DREAM-compromised plants. These findings establish the DREAM complex components as important regulators of the meiotic program in plants. Given that DREAM dysfunction causes reproductive defects in animals, this regulatory role may be conserved across multicellular eukaryotes.

INTRODUCTION

The DREAM complex is an ancient transcriptional regulator across eukaryotes, with conserved components spanning from humans to flowering plants (*1*–*5*). Pioneering studies in *Caenorhabditis elegans*, *Drosophila*, and mammalian cells revealed a conserved and crucial role of the DREAM complex [named after dimerization partner (DP), RB-like, E2F, and MuvB core] in regulating genes involved in cell cycle and development (*2*). In mammals, the complex operates in functionally distinct forms: The canonical repressive DREAM complex (MuvB, DP, Rb-like, E2F) silences cell cycle genes during quiescence, while the activator complexes MuvB-Myb (MMB) and MuvB-FOXM1 drive gene expression during S phase and mitosis, respectively (*6*, *7*). The capacity to act as both a transcriptional repressor and activator is a conserved property of the complex, as also demonstrated in *Drosophila*, where the dREAM/MMB complex exhibits both positive and negative activities on distinct target gene sets in proliferating cells (*8*).

Recently, the full complement of the animal DREAM complex has been identified in the flowering plant *Arabidopsis*, including homologs of the MuvB-core components LIN9 known as ALWAYS EARLY (ALY1, ALY2, and ALY3), the LIN54/TESMIN/TSO1-LIKE CXC homologs (TCX5 and TCX6), homologs of LIN52 (LIN52A and LIN52B), and homologs of ABNORMAL CELL LINEAGE PROTEIN 37 (LIN37A and LIN37B) (*3*, *4*, *9*). In addition, plant-specific components have been identified, including BTE1/DRC2, which mediates DREAM-dependent transcriptional repression by antagonizing H3K4me3 deposition at target gene promoters (*3*, *10*, *11*), but it is currently not clear to what extent there are different DREAM/MuvB complexes with specific cell cycle or developmental roles. In plants, the activator/repressor switch operates through MYB3R transcription factors. MYB3R4 acts as a transcriptional activator, while MYB3R3 and MYB3R5 act as repressors, forming distinct DREAM-like complexes in a mutually exclusive manner (*9*). Notably, no plant homologs of B-Myb and FOXM1 have been identified, suggesting that the plant DREAM complex achieves activator/repressor switching through a distinct mechanism compared to animals (*1*, *9*). Functional studies have shown that the *Arabidopsis* DREAM complex transcriptionally represses genes related to the cell cycle and maintenance of DNA methylation in somatic tissues (*4*, *9*). In addition, it was found to restrict plant growth following DNA damage (*3*).

Whether the DREAM complex plays any role in reproductive development and meiosis in plants, however, has remained unexplored. Given that DREAM dysfunction causes fertility defects across animals (*8*, *12*–*15*) and that precise transcriptional control of meiotic gene expression is essential for faithful recombination and chromosome segregation, we investigated whether the DREAM complex regulates meiotic gene expression in *Arabidopsis*. Here, we show that core DREAM complex components ALY1, ALY2, TCX5, and TCX6 are required for crossover (CO) formation, that TCX5 directly binds and regulates key meiotic recombination genes including *MER3*, and that it acts as both a transcriptional repressor and activator in a tissue-specific manner.

RESULTS

DREAM mutants exhibit meiotic defects that compromise fertility

To explore a possible role of the DREAM complex in reproductive development, we analyzed single mutants of the core MuvB components, i.e., *aly1*, *aly2*, *aly3*, *tcx5*, *tcx6*, *lin37a*, *lin37b*, *lin52a*, and *lin52b* (fig. S1). As none of them differed notably from wild-type (WT) plants, we generated double mutants of presumed redundant components. While *lin37a/b*, *lin52a/b*, *aly1/3*, and *aly2/3* double mutants were indistinguishable from WT, *aly1/2* and *tcx5/6* mutants exhibited severe

[1]Department of Developmental Biology, University of Hamburg, 22609 Hamburg, Germany. [2]Institute of Science and Technology Austria, 3400 Klosterneuburg, Austria. [3]Institute of Plant Sciences-Paris-Saclay, 91190 Gif-sur-Yvette, France. [4]State Key Laboratory of Genetics and Development of Complex Phenotypes, Institute of Plant Biology, School of Life Sciences, Fudan University, Shanghai 200433, China. [5]Guangdong Basic Research Center of Excellence for Precise Breeding of Future Crops, Guangdong Laboratory for Lingnan Modern Agriculture, Guangdong Provincial Key Laboratory of Protein Function and Regulation in Agricultural Organisms, College of Life Sciences, South China Agricultural University, Guangzhou 510642, China.
*Corresponding author. Email: arp.schnittger@uni-hamburg.de
†Deceased on 20 July 2025.

Downloaded from https://www.science.org at Institute of Science & Technology Austria (ISTA) on November 17, 2026

sterility, with reduced seed sets (WT, 60 ± 0.4; *aly1/2*, 35 ± 1.8; *tcx5/6*, 11 ± 1.6; Fig. 1, A and B) and pollen viability (WT, 99.5 ± 0.2%; *aly1/2*, 91 ± 1.0%; *tcx5/6*, 86 ± 2.2%; $P < 0.0001$ for all comparisons against WT; Fig. 1, C and D).

Furthermore, both *aly1/2* and *tcx5/6* mutants displayed pollen size variation (Fig. 1C), hinting at gametophytic and/or meiotic defects. However, the transmission efficiency of *tcx6* was unaffected when *tcx5* homozygous/*tcx6* heterozygous plants were crossed with WT (male: 102%; female: 106%; table S1), indicating a sporophytic origin of the defects.

To assess whether female meiosis and male meiosis are differentially affected in *tcx5/6*, we performed reciprocal crosses between *tcx5/6* and WT plants and quantified seed set in F_1 siliques. Both crossing directions resulted in significantly reduced seed numbers compared to WT × WT crosses (WT × WT: 41.6 ± 5.9; *tcx5/6* × WT: 21.9 ± 8.3; WT × *tcx5/6*: 31.9 ± 11.4; $P < 0.0001$ and $P = 0.0152$, respectively, fig. S2, A and B). Notably, the reduction in seed set when *tcx5/6* was used as the male parent exceeds what would be expected from the 14% pollen viability alone, suggesting that a fraction of apparently viable *tcx5/6* pollen carries meiotic defects that only manifest as fertilization failure or early seed abortion. The seed set was more severely reduced when *tcx5/6* was used as the female parent, and the difference between the two crossing directions was significant ($P = 0.01$), suggesting that female meiosis is more strongly affected than male meiosis in *tcx5/6*. Consistent with this, chromosome spreads and 4′,6-diamidino-2-phenylindole (DAPI) staining of whole ovules revealed univalent formation at metaphase I in *tcx5/6* female meiocytes (fig. S2, C and D), demonstrating that female meiosis is also impaired in *tcx5/6*.

Given that male meiocytes are more experimentally accessible, we analyzed meiotic progression by chromosome spreads to characterize the underlying defects in detail. Both double mutants showed unpaired chromosomal regions at pachytene (Fig. 1E, g and m, arrowheads), whereas WT chromosomes were fully paired. Pairing defects are followed by incomplete synapsis at late pachytene (fig. S3A). At diakinesis and metaphase I, univalents were observed in the mutants (Fig. 1E, h, i, n, and o) instead of the five bivalents seen in WT (Fig. 1E, b and c). The average numbers of bivalence were 5.0 in WT, 3.8 in *aly1/2*, and 3.3 in *tcx5/6* ($n = 81$, 48, and 46, respectively; aberrant metaphase I cells showing chromosome entanglements were excluded from this calculation). At interkinesis, we identified lagging chromosomes and unbalanced chromosome pools (Fig. 1E, j, k, p, and r, white arrowheads), and after meiosis II, the formation of triads and polyads could be observed (Fig. 1E, l and s, and fig. S3B) instead of balanced tetrads as in WT (Fig. 1E, f).

These meiotic abnormalities indicated severe defects in recombination in DREAM complex mutants. The average number of chiasmata, the physical manifestation of CO, during metaphase I (Fig. 1F) was significantly reduced in both *aly1/2* (6.5 ± 0.5) and *tcx5/6* (5.3 ± 0.5) compared to WT (9.5 ± 1.7; $n = 59$, 47, 39; $P < 0.0001$ for all comparisons against WT). Notably, 11% of *aly1/2* and 15% of *tcx5/6* meiocytes lacked chiasmata entirely, demonstrating that the DREAM complex components ALY1/2 and TCX5/6 are important for CO formation and faithful chromosome segregation in *Arabidopsis*.

DREAM complex components are required for class I CO formation

To determine which step in the recombination pathway was impaired in DREAM mutants, we assessed meiotic double-strand break (DSB) formation. DSBs are catalyzed by the SPO11 complex (*16*, *17*) in the context of the chromosome axis, a proteinaceous structure, from which DNA loops emerge. The axis includes integral axis proteins such as ASYNAPTIC3 (ASY3) as well as axis-associated proteins such as ASY1 (*18*, *19*), which build a scaffold for SPO11. SPO11-mediated DSBs generate 3′ single-stranded DNA overhangs coated by RAD51 and DMC1 to promote strand invasion and joint molecule formation (*20*, *21*). Quantification of RAD51 foci at zygotene revealed no significant difference between *aly1/2*, *tcx5/6*, and WT [$P = 0.64$ for *aly1/2* versus WT and $P = 0.96$ for *tcx5/6* versus WT, one-way analysis of variance (ANOVA); fig. S3, C and D], suggesting that DSB formation and their initial processing are unaffected in *aly1/2* and *tcx5/6* mutants.

A subset of processed DSBs is resolved as COs by two pathways: class I and class II (*22*–*24*). Class I COs, which account for ~85% of total COs in *Arabidopsis*, rely on the so-called ZMM proteins such as MER3 (*25*), PTD (*26*), SHOC1 (*27*), ZIP4 (*28*), MSH4/5 (*29*), and HEI10 (*30*). Assessing class I COs by quantifying HEI10 foci in late pachytene revealed a significant reduction in *aly1/2* (6.2 ± 0.5) and *tcx5/6* (5.8 ± 0.6) compared to WT (10.0 ± 0.2; $n = 10$ for all genotypes; $P < 0.0001$ for all comparisons against WT; Fig. 1, G and H), indicating that ALY1/2 and TCX5/6 function is in particular required for class I CO formation.

To further dissect how CO formation pathways are affected in the DREAM mutant background, we generated genetic combinations of *tcx5/6* with key CO pathway components. Triple mutants of *tcx5/6 spo11-1* were indistinguishable from *spo11-1* single mutants, with both showing a complete absence of COs at metaphase I (Fig. 2, A and B), placing TCX5/6 function downstream of SPO11-1–dependent DSB formation.

To assess the contribution of class I COs to the residual CO formation in *tcx5/6*, we generated the *tcx5/6 msh4* triple mutant, which significantly reduced the average bivalence number from 3.2 in *tcx5/6* to 1.1 in the triple mutant ($P < 0.0001$, one-way ANOVA; Fig. 2), with the fraction of cells showing complete CO loss increasing from 15% in *tcx5/6* to 46% in *tcx5/6 msh4*. These results demonstrate that while class I CO formation is severely compromised in *tcx5/6*, a residual class I CO remains. Combining *tcx5/6* with *mus81* similarly reduced average bivalence numbers to 2.2, with 42% of cells showing complete CO loss, indicating that a fraction of the remaining COs in *tcx5/6* are class II/MUS81–dependent (Fig. 2, A and B). As *mus81* single mutants show bivalent numbers comparable to WT (5.0), the significant reduction of average bivalence number seen in *tcx5/6 mus81* compared to the *tcx5/6* background (2.2 and 3.2, respectively, $P < 0.0001$, one-way ANOVA) indicates that residual CO formation in *tcx5/6* becomes disproportionately dependent on the MUS81-dependent class II pathway.

To investigate whether ALY1/2 and TCX5/6 act in the same pathway, we generated the *aly1/2 tcx5/6* quadruple mutant. Notably, the quadruple mutant displayed a markedly enhanced CO loss phenotype compared to *tcx5/6*, with average bivalence dropping to 1.1 ($P < 0.001$, one-way ANOVA) and more than 60% of metaphase I cells showing a complete absence of COs (Fig. 2). This near-complete loss of CO formation demonstrates that MuvB activity is not completely abolished in neither *aly1/2* nor *tcx5/6* mutants, consistent with the finding that the *aly1/2/3* triple mutant is lethal (*4*). In addition, these results corroborate the involvement of a MuvB core–containing complex in controlling meiotic recombination in *Arabidopsis*.

Consistent with a function in meiosis, we found that ALY1, TCX5, and TCX6 localized to meiotic chromosomes, as revealed by genomic

Downloaded from https://www.science.org at Institute of Science & Technology Austria (ISTA) on November 17, 2026

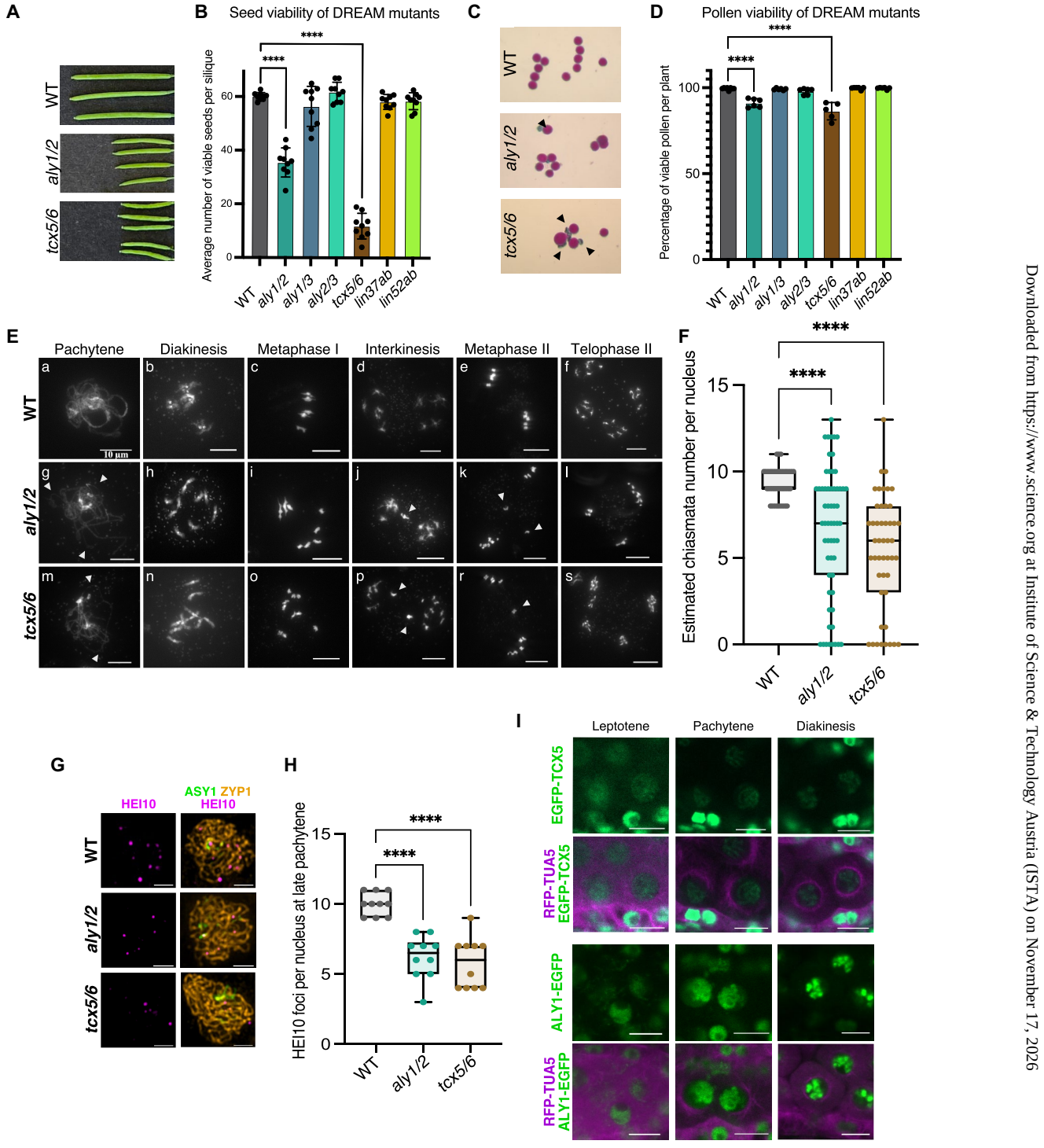


Fig. 1. The DREAM complex components are vital for successful meiosis. (**A**) The DREAM mutants *aly1/2* and *tcx5/6* show reduced length of siliques. (**B**) Seed viability of mutants of core DREAM components ($n = 10$ for all, $P < 0.0001$). (**C**) Pollen size variation and death observed in *aly1/2* and *tcx5/6*. Dead pollens are small and slightly blue-stained (black arrowhead). (**D**) Pollen viability for mutants of core DREAM components ($n = 10$ for all, $P < 0.0001$). (**E**) Meiotic stages in WT (a to f), *aly1/2* (g to l), and *tcx5/6* (m to s) double mutants were observed. Scale bars, 10 µm. (**F**) Estimated chiasmata numbers were calculated on the basis of metaphase I cells ($n = 40$, 47, and 59 for WT, *aly1/2*, and *tcx5/6* respectively; $P < 0.0001$). (**G**) HEI10 foci at late pachytene in WT, *aly1/2*, and *tcx5/6* mutants were observed via immunohistochemical staining of HEI10 (magenta), ASY1 (green), and ZYP1 (orange). Scale bars, 2 µm. (**H**) DREAM mutants exhibit a reduced number of HEI10 foci compared to WT ($n = 10$ for all; ****$P <$ 0.0001). A one-way ANOVA followed by Dunnett's multiple comparison test was used for (B), (D), (F), and (H). (**I**) ALY1-EGFP and EGFP-TCX5 (green) expressed in meiocytes and localized to chromosomes. RFP-TUA5 (magenta) serves as a meiotic stage marker. Scale bars, 10 µm.

Downloaded from https://www.science.org at Institute of Science & Technology Austria (ISTA) on November 17, 2026

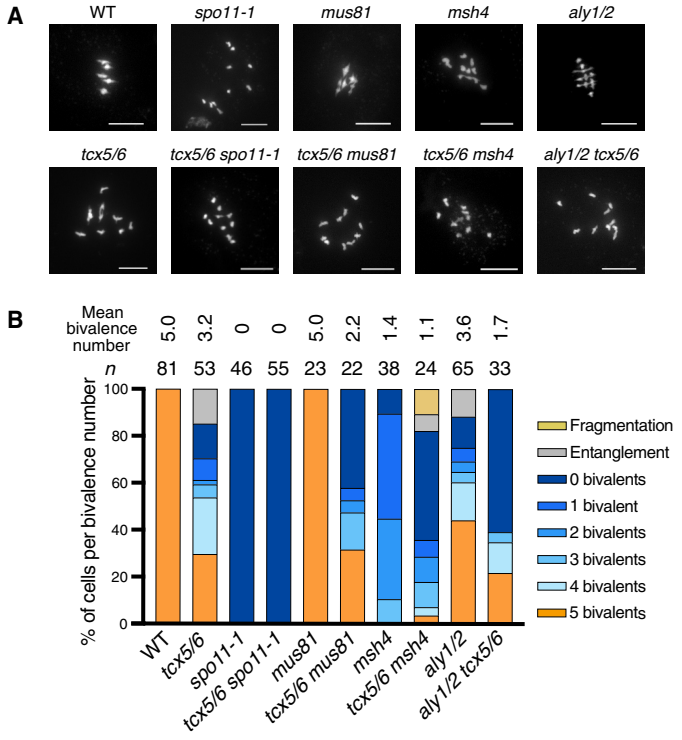


Fig. 2. ALY1/2 and TCX5/6 act downstream of DSB initiation to promote CO formation. (**A**) Representative images of metaphase I chromosomes in WT, *tcx5/6*, *spo11-1*, *tcx5/6 spo11-1*, *mus81*, *tcx5/6 mus81*, *msh4*, *tcx5/6 msh4*, *aly1/2*, and *aly1/2 tcx5/6*. Scale bars, 10 μm. (**B**) Stacked bar charts showing the proportion of metaphase I cells with zero to five bivalents and chromosome entanglements for each genotype. Mean bivalent numbers and cell counts (*n*) are indicated above each bar. Cells with chromosome entanglements and fragmentation were excluded from mean bivalent calculations.

reporter lines (Fig. 1I and fig. S4, A to C). Colocalization of TCX6 with the chromosome axis protein ASY3 confirms that DREAM complex components localize to meiotic chromosomes (fig. S4D). The enhanced green fluorescent protein (EGFP)-TCX5 reporter nearly completely restored fertility in *tcx5/6* (the average bivalent numbers from 3.3 to 5.0; fig. S5, A and B), validating its functionality. The ALY1-EGFP reporter largely rescued *aly1/2*, increasing bivalent numbers from 3.8 to 4.8, close to the WT level of 5.0 (fig. S5B), although residual meiotic defects suggest that ALY1-EGFP may not be fully functional.

Meiotic transcriptome analysis reveals deregulation of cell cycle and DNA repair genes

To pinpoint the genes responsible for the meiotic defects in *aly1/2* and *tcx5/6*, we compared the transcriptomes of male meiocytes from both mutant combinations with WT. Whole-transcriptome sequencing yielded more than 71 million reads per sample (three replicates per genotype), with >91% of the reads achieving 99.9% base-calling accuracy (table S2). A total of 17,775 genes were identified to be transcribed in WT, 17,840 in *aly1/2*, and 18,110 in *tcx5/6*. Of these, 17,176 genes were commonly expressed across all genotypes (Fig. 3A). Differential expression analysis revealed 655 up-regulated and 256 down-regulated genes in *aly1/2* and 1358 up-regulated and 685 down-regulated genes in *tcx5/6* compared to the WT (Fig. 3, B and C). The greater number and magnitude of gene expression changes in *tcx5/6* (Fig. 3, B and C, and table S3) correlate with its more severe meiotic defects relative to *aly1/2* (Fig. 1, F and H). Possibly, ALY3 partially compensates for the loss of ALY1/2, consistent with the embryonic lethality of *aly1/2/3* triple mutants (*4*).

To identify the biological pathways represented by the differentially expressed genes (DEGs), we performed a gene ontology (GO) enrichment analysis of the deregulated genes in *aly1/2* and *tcx5/6* compared to WT. Among the up-regulated genes, both mutants showed a significant enrichment for the GO term cell cycle, with 53 genes in *aly1/2* [false discovery rate (FDR) = 1.50×10^{-15}] and 123 in *tcx5/6* (FDR = 5.60×10^{-37}; Fig. 3, D and E), consistent with a conserved role of the DREAM complex in cell cycle regulation (*1*, *7*, *31*). In addition, GO terms related to DNA repair and DNA metabolic process are significantly enriched in *tcx5/6* [62 genes (FDR = 3.30×10^{-17}) and 104 genes (FDR = 5.10×10^{-27}), respectively; Fig. 3, D and E]. By contrast, GO enrichment analysis of the down-regulated genes did not identify any terms directly associated with the meiotic defects observed in the mutants (fig. S6).

To uncover the molecular basis of reduced COs in mutants of DREAM components, we focused on the expression of genes involved in meiotic recombination. Two observations may account for the CO defects: (i) up-regulation of CO-suppressing factors, such as FANCM, RECQ4A, and RMI1, and (ii) down-regulation of the CO-promoting factor MER3 (Table 1).

The CO-suppressing factor FANCM promotes DSB repair via synthesis-dependent strand annealing (*32*), while RECQ4A/B, being part of the RTR complex together with TOP3 α and RMI1, resolves double Holliday junctions into noncrossovers (NCOs) (*33*, *34*). Mutants in *FANCM*, *RECQ4*, and *RMI1* exhibit elevated CO numbers because of increased class II COs (*32*, *34*, *35*). Although up-regulation of these suppressors has not previously been associated with reduced CO levels, it is tempting to speculate that their elevated expression contributes to the CO defects observed in DREAM mutants.

MER3, a conserved eukaryotic helicase, promotes CO formation by catalyzing D-loop migration and double Holliday junction formation. Like other ZMM mutants, *mer3* exhibits decreased levels of COs, leading to univalent formation, recapitulating the defects seen in *aly1/2* and *tcx5/6* (*36*).

Together, our expression analyses of isolated mutant meiocytes revealed the deregulation of several central recombination regulators in the absence of core DREAM components. We hence hypothesized that the deregulation of one or likely more of these genes is the cause for the observed recombination defect in *aly1/2* and *tcx5/6*.

TCX5 directly binds promoters of cell cycle and DNA repair genes

To address whether the transcriptional deregulation of the above-identified meiotic recombination regulators in *aly1/2* and *tcx5/6* could be a result of the direct regulation by the DREAM complex components, we performed cleavage under targets and tagmentation (CUT&Tag) using anthers of plants harboring a functional EGFP-TCX5 reporter (fig. S5). This resulted in the identification of 3470 TCX5-enriched genes. Among these, 271 were up-regulated and 98 were down-regulated in *tcx5/6*, showing a significant overlap between TCX5-enriched targets and DEGs in the mutant ($P = 1.1 \times 10^{-25}$ and $P = 0.001$, respectively; Fig. 3F).

TCX5 CUT&Tag reads were predominantly enriched around transcription start sites (TSSs), as expected for DREAM complex binding

Downloaded from https://www.science.org at Institute of Science & Technology Austria (ISTA) on November 17, 2026

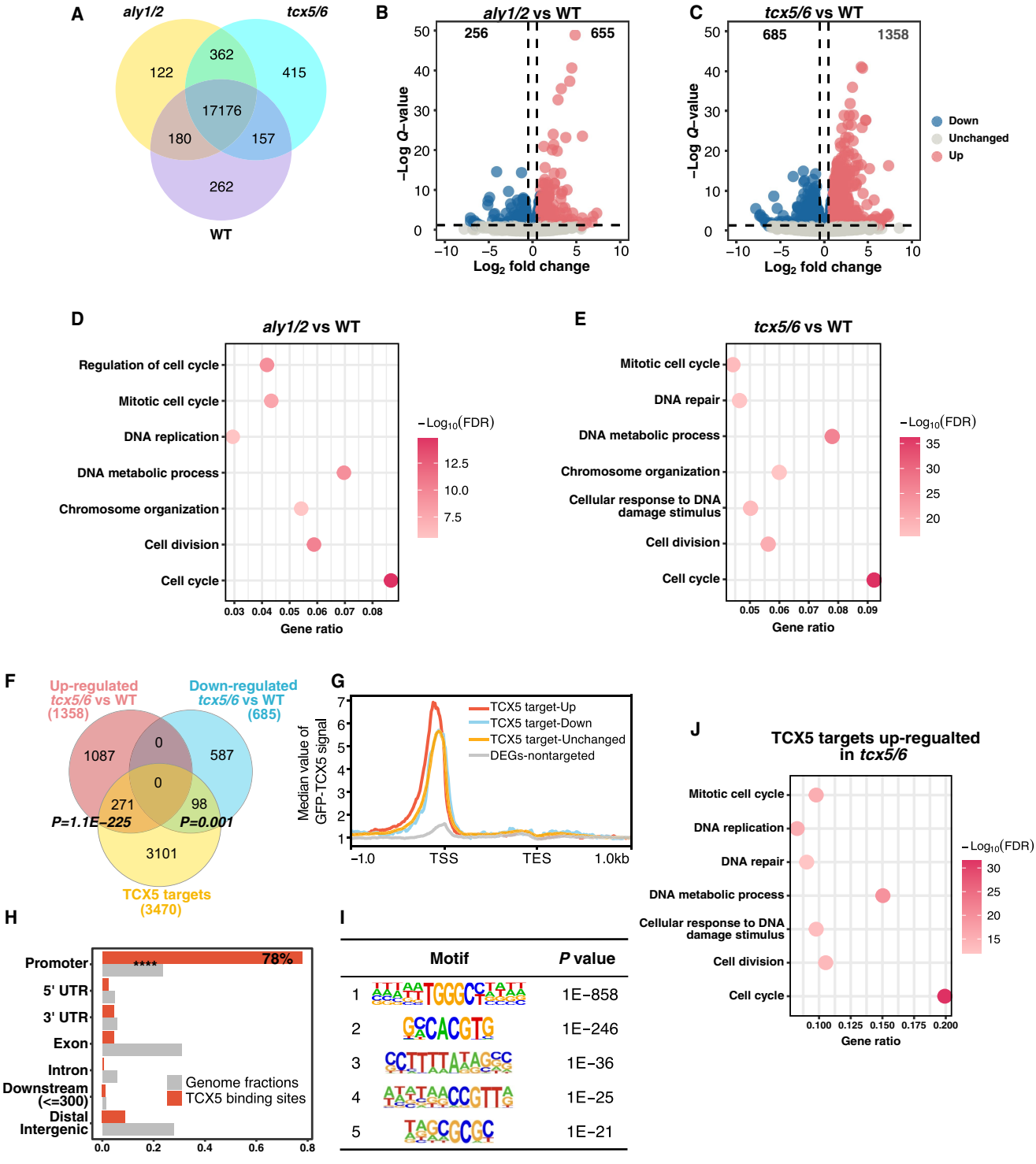


Fig. 3. Meiocyte transcriptome analyses of DREAM mutants and TCX5 binding analyses reveal DREAM-dependent regulation of cell cycle and DNA repair genes. (**A**) Venn diagram showing the number of genes expressed in WT, *aly1/2*, and *tcx5/6* male meiocytes. (**B** and **C**) Volcano plots of DEGs in *aly1/2* (B) and *tcx5/6* (C) relative to WT. (**D** and **E**) GO enrichment analysis of up-regulated genes in *aly1/2* (D) and *tcx5/6* (E), highlighting enrichment in pathways related to cell cycle and DNA repair. (**F**) Overlap between up-regulated genes (pink), down-regulated genes (blue) in *tcx5/6* male meiocytes, and TCX5 targets (yellow) identified by EGFP-TCX5 CUT&Tag in anthers (hypergeometric test: $P = 1.1 \times 10^{-25}$ and $P = 0.0001$). (**G**) Meta-plot showing the median EGFP-TCX5 CUT&Tag signal across gene bodies for up-regulated (pink), down-regulated (blue), nondifferentially expressed (yellow), and nontargeted (gray) DEGs. TSS, transcription start site; TES, transcription end site. (**H**) Distribution of TCX5 binding sites, with predominant promoter association (<1 kb from TSS; hypergeometric test, ****$P < 0.0001$). (**I**) HOMER motif analysis of promoter-bound TCX5 sites identifies a GC-rich motif (1), a G-box motif (2), and motifs recognized by Tesmin/TSO1–like CXC-domain proteins (3), E2Fs (4), and MYB3Rs (5). (**J**) GO enrichment of TCX5 targets up-regulated in tcx5/6 male meiocytes.

Downloaded from https://www.science.org at Institute of Science & Technology Austria (ISTA) on November 17, 2026

Table 1. Differential expression of recombination pathway genes in *aly1/2* and *tcx5/6* meiocytes. Log_2(fold change) values and adjusted *P* values (P_{adj}) are shown for each gene, together with annotated gene functions.

		aly1/2 vs WT		*tcx5/6* vs WT		
Gene ID	**Name**	**Log_2(fold change)**	**P_{adj}**	**Log_2(fold change)**	**P_{adj}**	**Function**
AT3G27730	MER3	−0.8870	0.0454	−0.9107	0.0029	ZMM protein
AT1G35530	FANCM	0.6340	0.0788	1.2987	9.3E−08	Anti-CO factor
AT1G10930	RECQ4A	0.6771	0.0091	0.9473	3.3E−06	Anti-CO factor
AT5G63540	RMI1*	0.3216	0.5545	0.8594	0.0041	Anti-CO factor
AT3G22880	DMC1	0.8584	0.0012	0.6823	0.0152	DSB processing

*Deregulation of *RMI* is observed only in *tcx5/6* meiocytes, whereas its transcript levels are not significantly altered in *aly1/2* relative to WT.

(Fig. 3, G and H, and fig. S7A) (*4*, *8*, *12*, *37*). HOMER motif enrichment analysis of these regions identified several overrepresented motifs, with the most enriched being the GC-rich motif ($P = 1 \times 10^{-858}$), followed by a G-box motif ($P = 1 \times 10^{-246}$; Fig. 3I). We also detected motifs recognized by tesmin/TSO1–like CXC domain–containing proteins ($P = 1 \times 10^{-36}$), E2Fs ($P = 1 \times 10^{-21}$), and MYB3Rs ($P = 1 \times 10^{-25}$; Fig. 3I), which have been shown to be plant DREAM–associated transcription factors (*3*, *4*).

A GO term enrichment analysis of genes both TCX5-enriched and up-regulated in *tcx5/6* revealed significant enrichment for categories related to DNA repair and cell cycle (Fig. 3J), while TCX5-enriched and down-regulated genes in *tcx5/6* did not yield GO terms obviously related to the observed meiotic defects (fig. S7B). Reflecting shared meiotic defects of *aly1/2* and *tcx5/6*, 141 of the 655 genes up-regulated in *aly1/2* were direct TCX5 targets, and 119 of these were up-regulated in *tcx5/6* (fig. S7, C and D). GO term enrichment analysis of these 119 genes similarly highlighted cell cycle and DNA repair categories (fig. S7E).

Notably, we found no evidence of TCX5 binding at the promoter of *FANCM*, indicating that its up-regulation is unlikely to be directly mediated by TCX5. In contrast, TCX5 was detected at the promoter of *RECQ4A* and *RMI1* (table S3). While *RECQ4A* expression was found to be increased in *tcx5/6* and in *aly1/2* meiocytes, *RMI1* transcript levels were only elevated in *tcx5/6* meiocytes (Table 1). In addition, no transcriptional up-regulation was observed for *TOP3α*, the third core component of the RTR complex (table S3). These findings suggest that the RTR complex is unlikely to account for the reduced COs observed in *aly1/2* and *tcx5/6*.

Transcriptional activation of *MER3* by DREAM components promotes CO formation

Among the TCX5-bound genes differentially expressed in DREAM mutants, the down-regulation of the CO-promoting helicase *MER3* stood out as a candidate directly linking TCX5 activity to reduced CO formation. To test whether *MER3* down-regulation functionally contributes to the CO defects in DREAM mutants, we first characterized TCX5 binding at the *MER3* promoter in detail. TCX5 binding was detected 315 base pairs (bp) upstream of the *MER3* start codon (Fig. 4A), and within this peak region, we identified the TCX/CXC-domain binding motif found in this study, as well as motifs recognized by MYB3R and E2F transcription factors and the previously described TCX5 binding motif (*4*).

To assess the functional importance of this TCX5-bound region for *MER3* transcriptional regulation, we performed a transient dual-luciferase assay in tobacco leaves using different versions of the *MER3* promoter fused to a luciferase reporter, with TCX5 and TCX6 as effectors (Fig. 4B). When TCX5 and TCX6 were coexpressed, the full *MER3* promoter (1016 bp upstream of the start codon) showed a significant reduction in luciferase signal ($P < 0.001$, one-way ANOVA), while TCX5 alone showed a reduction trend that did not reach statistical significance ($P = 0.06$), suggesting that TCX5 and TCX6 act cooperatively to repress *MER3* transcription (Fig. 4C). A promoter fragment containing only the TCX5 peak region was sufficient to recapitulate this down-regulation, demonstrating that TCX5 binding to this region is sufficient to mediate repression. Conversely, deletion of the TCX5 peak from the full promoter resulted in significantly elevated luciferase signal ($P < 0.0001$) compared to the 1016-bp promoter, confirming that this region is necessary for full repression. Consistently, a short promoter version (315 bp upstream) lacking the TCX5 peak and any TCX binding motifs similarly showed significantly elevated luciferase activity ($P < 0.0001$; Fig. 4C). Together, these results establish that the TCX5-bound region in the *MER3* promoter is both necessary and sufficient for TCX5/TCX6–mediated transcriptional regulation. We note that because this experiment was performed in tobacco leaves, which lack a meiotic context, it reflects the repressive function of the DREAM complex characteristic of somatic tissues. Nevertheless, it directly demonstrates that TCX5 and TCX6 bind and functionally regulate the *MER3* promoter through this specific region, supporting the conclusion that *MER3* is a direct transcriptional target of the DREAM complex components TCX5 and TCX6.

Having established that the TCX5-bound region in the *MER3* promoter is functionally important for its transcriptional regulation, we next sought to directly test whether *MER3* down-regulation contributes to the CO defects observed in DREAM mutants. We therefore generated a construct in which the genomic sequence of *MER3* fused to *EGFP* was driven by the meiosis-specific *DMC1* promoter. Notably, *DMC1* expression was up-regulated in *aly1/2* and *tcx5/6*, suggesting that the *DMC1* promoter might confer a strong expression of *MER3* in meiocytes (Fig. 5A and Table 1).

We observed that MER3-EGFP localization was confined to male meiocytes (Fig. 5B), and the *pDMC1-MER3-EGFP* construct fully restored recombination in homozygous *mer3* mutants (Fig. 5, C and D, and fig. S8A), validating its functionality. We next introduced this construct into $tcx5^{-/-}$ $tcx6^{+/-}$ and $aly1^{-/-}$ $aly2^{+/-}$ mutants to assess whether increased *MER3* expression could restore CO formation defects. In contrast to its meiocyte-restricted localization in *mer3*, MER3-EGFP was additionally detected in the tapetal cells surrounding the

Downloaded from https://www.science.org at Institute of Science & Technology Austria (ISTA) on November 17, 2026

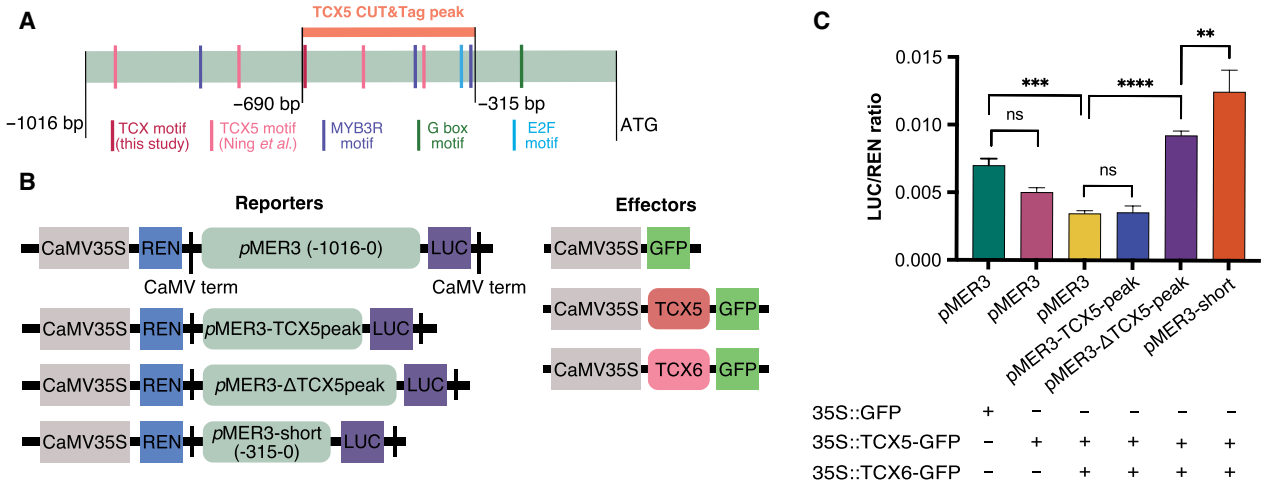


Fig. 4. The DREAM complex component TCX5 binds the *MER3* promoter and regulates its transcription. (**A**) Schematic of the *MER3* promoter showing the position of the TCX5 CUT&Tag peak region (highlighted in orange) and identified binding motifs, including the TCX motif identified in this study, the previously described TCX5 motif (*4*), MYB3R motif, G-box motif, and E2F motif. (**B**) Schematic of reporter and effector constructs used in the dual-luciferase assay. Reporters consist of different versions of the *MER3* promoter driving LUC, with REN under the CaMV 35*S* promoter as an internal control. Effectors consist of TCX5-GFP and TCX6-GFP under the CaMV 35*S* promoter. (**C**) Dual-luciferase reporter assay in tobacco leaves showing LUC/REN ratios for each promoter construct in the presence of the indicated effectors. Error bars indicate standard deviation. Statistical analysis was performed using a one-way ANOVA followed by Tukey's multiple-comparison test. $^{**}P < 0.01$; $^{***}P < 0.001$; $^{****}P < 0.0001$; ns, not significant.

meiocytes in both *aly1/2* and *tcx5/6* anthers (Fig. 5B and fig. S8B). Given that *DMC1* is a direct TCX5 target (Fig. 5A) and TCX5 binding is lost in DREAM mutants, this ectopic tapetal expression reflects the derepression of the *DMC1* promoter in somatic anther cells upon loss of DREAM function, consistent with its canonical repressive role in somatic tissues (*4*, *9*). This observation directly demonstrates that the DREAM complex restricts *DMC1* promoter activity, and potentially that of other meiotic genes, to meiocytes within the anther, thereby enforcing the spatial specificity of meiotic gene expression.

Notably, *MER3-EGFP* expression in *aly1/2* increased the proportion of meiocytes with five bivalents from 40 to 55% (Fig. 5C), and cells exhibiting two, one, or no bivalents were no longer observed. *MER3-EGFP* expression in *tcx5/6* reduced the fraction of cells with no bivalents from 15 to 1% and those with one bivalent from 9 to 4% (Fig. 5C). Furthermore, *MER3-EGFP* expression significantly increased the average bivalent numbers from 3.8 to 4.8 in *aly1/2* ($P < 0.0001$) and from 3.3 to 4.1 in *tcx5/6* ($P < 0.008$; Fig. 5, C and D, e and g). However, it also elevated the incidence of chromosome entanglements, potentially contributing to the chromosome fragmentation seen in anaphase I (Fig. 5D, l and n). The partial but significant rescue of CO formation identifies *MER3* as a major, although not the sole, target of the DREAM complex components in meiosis and suggests that additional targets of these components contribute to the full complement of COs in *Arabidopsis*.

The meiotic DREAM complex has a specialized configuration

Seeing that ALY1/2 and TCX5/6 directly promote the expression of *MER3* in meiocytes and that, conversely, the restoration of *MER3* expression profoundly promotes a WT-like recombination pattern in *aly1/2* and *tcx5/6* mutants indicated that ALY1/2 and TCX5/6 not only have repressive but also activating functions in meiocytes. Previous work has indicated that the three-repeat MYB proteins MYB3R1 and MYB3R4 are part of an activating DREAM complex in *Arabidopsis* in a manner analogous to FOXM1-containing complexes. We therefore analyzed *myb3r1/4* double mutants but did not observe any recombination defects similar to *aly1/2* and *tcx5/6* mutants (fig. S9, A and B). We then wondered whether bona fide repressive components genetically contribute to the defects seen in *aly1/2* and *tcx5/6* mutants. Therefore, we also analyzed triple mutants in the repressively acting MYBs (*myb3r1/3/5*) but again did not observe recombination defects (fig. S9, A and B). Last, we also generated transgenic plants in which we mutated the previously found RBR1-binding LxCxE motif (*3*) to AxAxA in the genomic TCX5/6 reporter. Notably, expression of these versions fully restored a WT-like meiotic phenotype in *tcx5/6* mutants (fig. S9, B to E). Thus, it seems likely that ALY1/2 and TCX5/6 participate in a specialized DREAM complex in meiosis that neither contains the known activating nor the established repressive components of the canonical somatic DREAM complex.

The DREAM complex components act as a context-dependent transcriptional repressor and activator

In animals, the DREAM core complex has been shown to act as both a transcriptional repressor and activator depending on the developmental context (*8*, *12*). Our data now reveal that DREAM complex components function as both transcriptional repressors and activators in male meiocytes. To explore this dual role, we integrated our meiocyte transcriptome data with previously published *tcx5/6* and WT seedling transcriptome data (*4*), together with TCX5 binding profiles obtained from seedlings [chromatin immunoprecipitation sequencing (ChIP-seq)] (*4*) and anthers (CUT&Tag; this study). We identified 1011 shared TCX5 target genes, with 2459 and 1732 genes uniquely bound in anthers and seedlings, respectively (fig. S10A). Among genes up-regulated in *tcx5/6* meiocytes and seedlings, 126 were common TCX5 targets enriched for cell cycle–related GO terms,

Downloaded from https://www.science.org at Institute of Science & Technology Austria (ISTA) on November 17, 2026

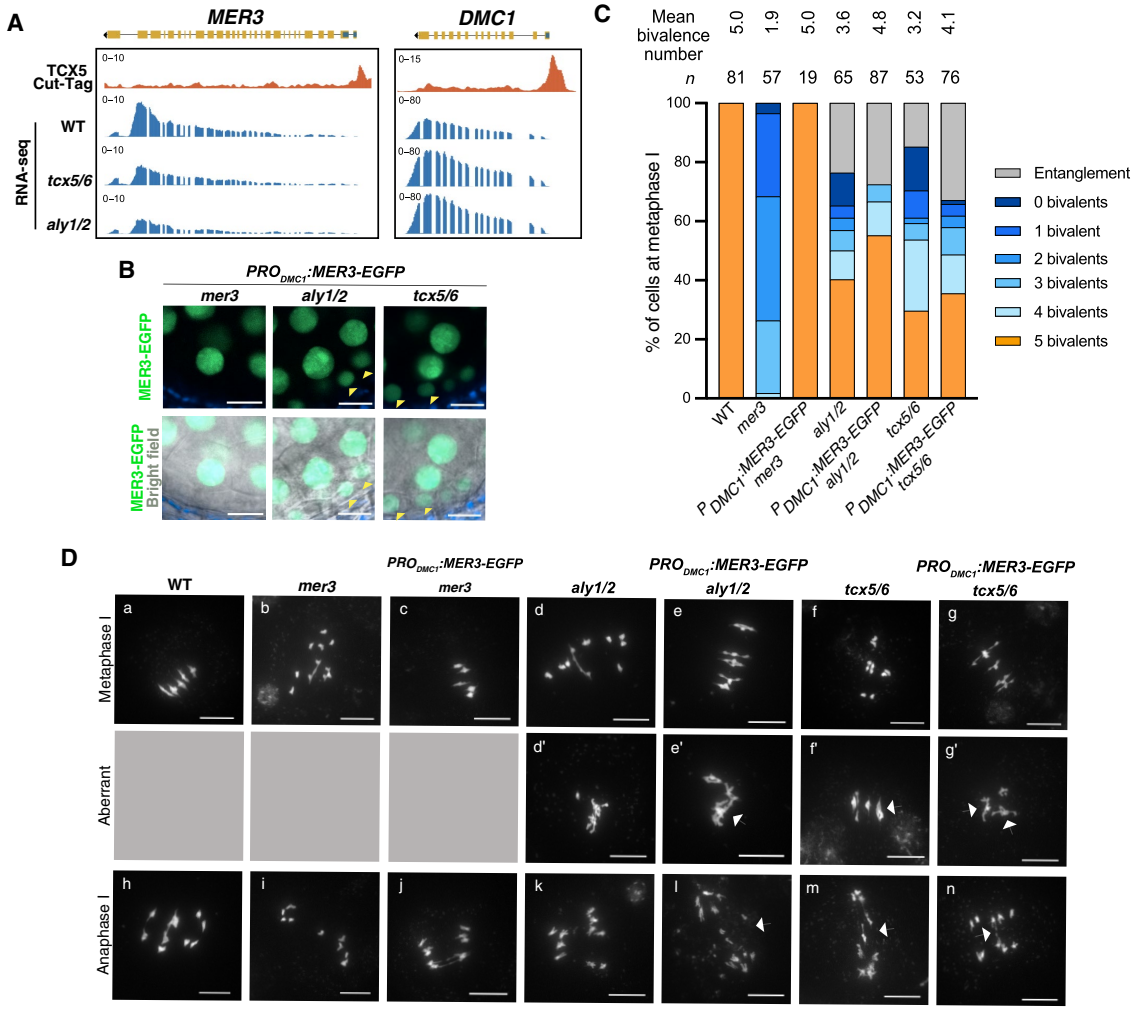


Fig. 5. The DREAM complex components activate *MER3* transcription to ensure proper CO formation. (**A**) Genome browser snapshot of *MER3* and *DMC1* transcript levels derived from RNA-seq in WT, *tcx5/6*, and *aly1/2* male meiocytes (blue tracks), aligned with the CUT&Tag signal for EGFP-TCX5 in anthers (dark orange track). (**B**) MER3-EGFP localization at anthers of PRO_{DMC1}*:MER3:EGFP mer3*, PRO_{DMC1}*:MER3:EGFP aly1/2*, and PRO_{DMC1}*:MER3:EGFP tcx5/6*. The first row shows the MER3-EGFP signal in green and autofluorescence in dark blue. The second row shows a merged image with a bright field to determine the cell shape. Yellow arrowheads indicate the MER3-EGFP signal at tapetal cells. Scale bars, 10 μm. (**C**) Frequency distribution of bivalent numbers and chromosome entanglement observed at metaphase I. "*n*" indicates the number of metaphase I cells analyzed and the mean bivalent number for each genotype. Cells displaying chromosome entanglement were excluded from the calculation of mean bivalent number. (**D**) Representative images of metaphase I and anaphase I chromosomes for each genotype: WT (a and h), *mer3* (b and i), PRO_{DMC1}*:MER3:EGFP mer3* (c, c′, and j), *aly1/2* (d, d′, and k), PRO_{DMC1}*:MER3:EGFP aly1/2* (e, e′, and l), *tcx5/6* (f, f′, and m), and PRO_{DMC1}*:MER3:EGFP tcx5/6* (g and n). White arrowheads mark chromosome entanglement at metaphase I (d′, e′, f′, and g′) and chromosome fragmentation at anaphase I (l, m, and n). Scale bars, 10 μm.

consistent with the conserved repressive role of the DREAM complex (fig. S10, B and C) (*1*, *37*, *38*). In contrast, TCX5-bound genes showed no significant overlap with genes down-regulated in *tcx5/6* seedlings (fig. S10D), whereas a large overlap exists in *tcx5/6* male meiocyte down-regulated genes and TCX5-bound genes in anthers (Fig. 3F). Moreover, no down-regulated genes in *tcx5/6* meiocytes and seedlings were shared TCX5 targets (fig. S10E). These findings led to the interesting hypothesis that TCX5's activating role is specific to reproductive tissues.

We note that this comparison integrates CUT&Tag data from anthers with ChIP-seq data from seedlings, and the difference in experimental technique may limit direct interpretation of differences in binding profiles. However, CUT&Tag data have been shown to recover the strongest and most functionally relevant ChIP-seq peaks with equivalent biological enrichments (*39*), supporting the biological relevance of the tissue-specific differences we observe.

Regulatory framework for meiotic gene expression controlled by DREAM complex components

To further explore the role of the DREAM complex components in reproductive development, particularly in meiosis, we examined 135 genes with established meiotic functions that are transcriptionally active in meiocytes (table S3). To this end, we assessed their transcriptional regulation and TCX5 binding in seedlings (*4*) and meiocytes/anthers. In seedlings, TCX5 binds to 93 of these genes. Of these, 84 were transcriptionally repressed in DREAM complex mutants, including key regulators of class I and II CO formation, DSB formation and repair, and synaptonemal complex assembly (table S3).

Downloaded from https://www.science.org at Institute of Science & Technology Austria (ISTA) on November 17, 2026

These results suggest that the DREAM complex broadly represses meiotic gene expression in nonreproductive tissues, confining their activation to the appropriate developmental context. This finding is consistent with an accompanying paper by Guo *et al.* (*40*) that shows that the DREAM complex represses meiotic recombination in somatic cells.

To then analyze the transcriptional regulation of these 135 genes in reproductive tissues, we adopted a more permissive cutoff for TCX5 enrichment, i.e., fold change >2 versus >4 used in the genome-wide CUT&Tag analysis. This approach accounts for the low proportion of meiocytes in anther tissue, which may dilute meiocyte-specific signals. Nonetheless, we cannot fully exclude the fact that some TCX5 binding sites unique to meiocytes may remain undetected.

In reproductive tissues, we identified five distinct regulatory patterns that illustrate how the DREAM complex components control reproductive gene expression (Fig. 6, A and B, and table S3): (i) Fourteen genes were not bound by TCX5 in neither anthers nor seedlings, indicating that they are not TCX5 targets in either context. (ii) Sixteen genes were not bound by TCX5 in anthers but were bound (and either repressed or unregulated) in seedlings, including the ZMM genes *HEI10* and *MSH5*, suggesting their release from DREAM-mediated repression in reproductive tissues. This pattern supports the above observation that the canonical DREAM complex is a key regulator of reproduction-specific gene expression. (iii) Fifty-nine genes were bound by TCX5 in anthers but not differentially expressed in meiocytes, such as *ASY1* and *ASY3* (chromosome axis formation) as well as *SPO11-1* and *SPO11-2* (DSB initiation). Possibly, these genes represent canonical DREAM complex targets whose expression is suppressed in the somatic cells of the anther but is already derepressed in meiocytes. Consequently, loss of TCX5/6 function would not further alter their expression in meiocytes, as the repression would already be lifted. (iv) Forty-four genes were bound by TCX5 in anthers and repressed in meiocytes, including *RAD51*, *X-RAY REPAIR CROSS COMPLEMENTING 3* (*XRCC3*),

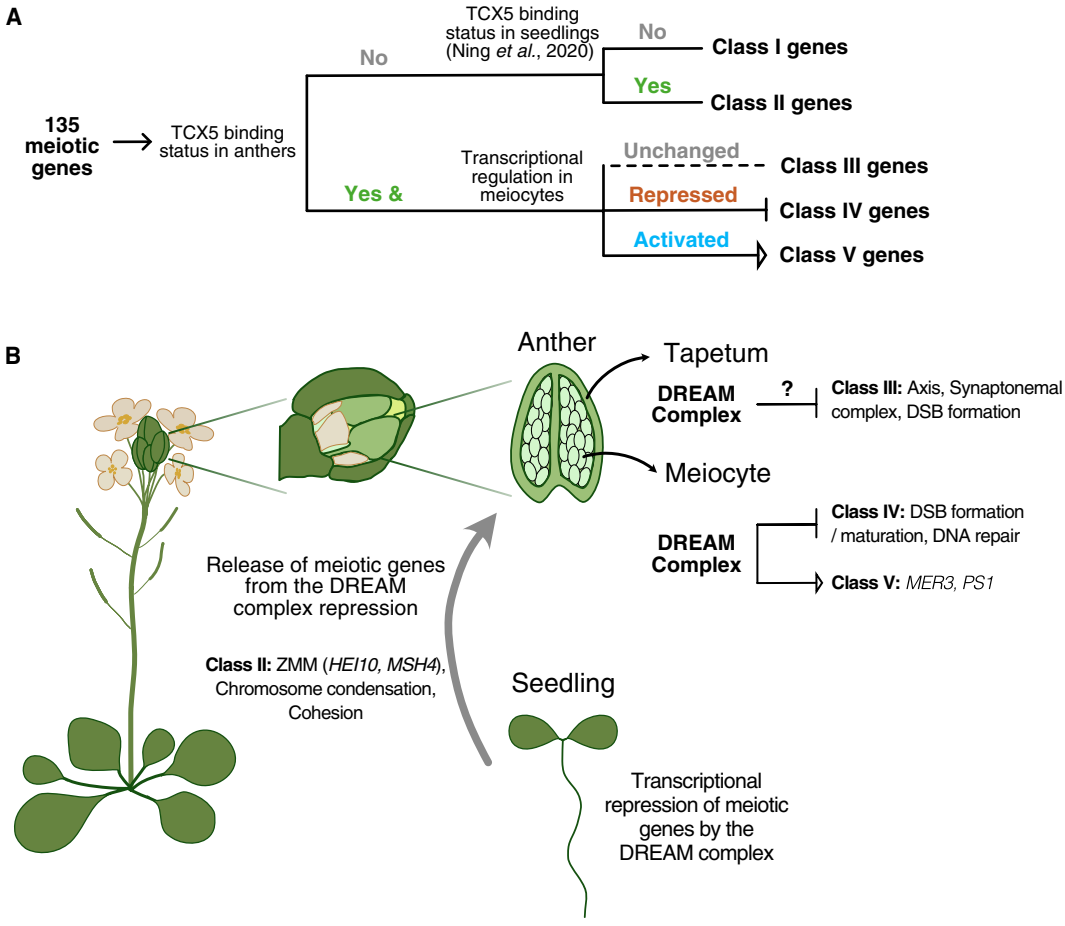


Fig. 6. DREAM complex–mediated regulation of meiotic genes. (**A**) Classification of 135 meiotic genes with established meiotic roles that are expressed in meiocytes. Class I: no TCX5 enrichment in either seedlings or anthers, indicating they are not direct DREAM targets. Class II: not bound by TCX5 in anthers but bound in seedlings; their transcription is repressed or unchanged in both seedlings and meiocytes. Class III: enriched for TCX5 binding in anthers but with no transcriptional changes in meiocytes. Class IV: TCX5-bound in anthers and transcriptionally repressed in meiocytes. Class V: TCX5-bound in anthers and transcriptionally activated in meiocytes. (**B**) Hypothetical model of DREAM-mediated regulation of meiotic genes across somatic and reproductive tissues. In seedlings, meiotic gene expression is repressed by the DREAM complex. In reproductive tissues, class II genes are derepressed, indicating reprogramming toward a reproductive state. Class III genes appear regulated at the anther level rather than in meiocytes, potentially restricting their expression to meiocytes. The repression of class IV genes in meiocytes suggests phase-specific control that confines their expression to a particular stage of meiosis and/or spatial restriction to meiocytes. Class V genes, *MER3* and *PS1*, highlight an unusual activator function of the DREAM complex in reproductive tissue.

Downloaded from https://www.science.org at Institute of Science & Technology Austria (ISTA) on November 17, 2026

MEIOSIS DEFECTIVE 1 (*MEI1*), *RMI1*, and *RECQ4A* (table S3). These are largely associated with DNA repair (*41*, *42*) and may be subjected to phase-specific regulation, e.g., during DSB formation and initial repair in leptotene and zygotene. Notably, *DMC1* also falls into this category. As shown above, the loss of TCX5/6 causes both the ectopic expression of *DMC1* in the anther tissues surrounding the meiocytes and its up-regulation within the meiocytes (Fig. 5, A and B). Class IV therefore may encompass two regulatory modes: temporal repression (e.g., *DMC1* down-regulation after early prophase) and spatial restriction to meiocytes, reflecting the multiple mechanisms through which TCX5 governs development-specific gene expression. (v) Two genes, *MER3* and *PS1*, the latter of which is important for proper meiotic spindle formation (*43*), were bound by TCX5 in anthers and transcriptionally activated in meiocytes. Given MER3's essential role in class I CO formation, this highlights an activator function of the DREAM complex components in reproductive tissue and suggests a direct link to the control of key meiotic processes.

DISCUSSION

Here, we identify the DREAM complex components ALY1/2 and TCX5/6 as transcriptional regulators of meiotic gene expression in *Arabidopsis*. A key target of their action is *MER3*. Partial restoration of bivalent formation by *MER3* expression, particularly in *tcx5/6*, suggests that additional targets of these components contribute to meiotic recombination. Moreover, the chromosome entanglements seen in particular in *tcx5/6* further implicate ALY1/2 and TCX5/6 in broader meiotic functions.

Notably, no transcription factor has yet been found that directly controls meiotic gene expression in *Arabidopsis* or any other plant species. Our work shows that the DREAM complex components ALY1/2 and TCX5/6 function as both a repressor and activator of transcription during reproduction. Their repressive role is consistent with prior studies in somatic tissues of *Arabidopsis* (*3*, *4*, *40*) and with the conserved function of DREAM complexes in other species (*37*, *38*, *44*). Together with Guo *et al.* (*40*), our work highlights that the DREAM complex represses a large subset of meiotic genes in somatic cells (e.g., seedlings), mirroring the somatic repression of germline genes observed for dREAM in *C. elegans* (*38*, *40*, *45*). Furthermore, in the reproductive context, the DREAM complex components fine-tune gene expression within anthers, restricting the expression of recombination genes, including *DMC1*, specifically to meiocytes. Possibly, this repression is even crucial to establish temporal regulation during meiosis, for example, restricting the expression of recombination genes to meiotic prophase I.

We uncover that DREAM complex components activate key meiotic genes, including *MER3*, and this activator role appears to be specific for reproductive processes, raising the possibility of a specialized DREAM variant in reproduction. In somatic tissues, the *Arabidopsis* DREAM complex switches between repressor and activator states through MYB3R transcription factors, with MYB3R3/5 acting as a repressor and MYB3R4 as an activator (*9*).

However, neither *myb3r1/4* activator nor *myb3r1/3/5* repressor mutants display CO defects (fig. S9, A and B), suggesting that MYB3Rs are not involved in TCX5/6- and ALY1/2-mediated meiotic gene regulation. Furthermore, TCX5/6 variants carrying mutations in the RBR1-binding LxCxE domain do not exhibit meiotic defects (fig. S9, B and C), indicating that TCX5/6 and RBR1 interaction is dispensable for meiotic gene regulation. However, we cannot exclude the possibility that RBR1 participates in a meiotic DREAM variant through alternative interaction interfaces or via other complex components. These mutant variants are properly expressed and show the same meiotic localization pattern as their respective WT proteins (fig. S9, D and E).

Together, these results further highlight the possibility that a specialized DREAM complex variant, distinct in composition from the canonical somatic complex, governs meiotic gene expression in reproductive tissues. The composition of such a variant and its potential meiosis-specific interactors remain to be determined.

Notably, the DREAM-like complexes are required for fertility across different animals, e.g., *C. elegans*, *Drosophila*, and mice (*8*, *12*–*15*). In mice, the testis-specific TCX5 homolog TESMIN/METALLOTHIONIEN-LIKE 5 (MTL5) interacts with LIN9, LIN37, and MYBL1, forming the MYBL1-MuvB complex (*46*); loss of either TESMIN and MYBL1 causes male sterility resulting from pachytene arrest, and MYBL1 was shown to activate genes involved in male meiosis (*47*). In *Drosophila*, the testis Meiotic Arrest Complex (tMAC), a testis-specific paralog composed of dREAM components alongside testis-specific factors, activates genes essential for the G_2/meiosis I transition and spermatid differentiation in primary spermatocytes, while the canonical dREAM complex represses genes not expressed in spermatocytes (*13*, *44*, *48*–*51*). This division of labor between a canonical repressive complex and a reproductive tissue-specific activating variant is notably analogous to what we propose here for *Arabidopsis*.

In *C. elegans*, the DRM complex, a functional analog of DREAM, regulates germ line–specific transcriptional programs (*12*, *45*), and its loss results in sterility and ectopic germ line–like expression of DNA repair genes in somatic cells (*38*). A complementary study by Guo *et al.* (*40*) now directly demonstrates this phenomenon in *Arabidopsis*: TCX5/6 repress meiotic DSB-formation genes in somatic tissues through limiting H3K4me3 deposition at their promoters, and loss of this repression leads to ectopic DSB formation and genomic instability. Consistent with this, our data show that the DREAM complex restricts *DMC1* promoter activity to meiocytes; when *MER3* is expressed under the *DMC1* promoter, ectopic expression of *MER3-EGFP* in tapetal cells is observed in *aly1/2* and *tcx5/6* but not in WT.

In summary, our study identifies a possible DREAM complex variant as a key transcriptional regulator of meiotic gene expression in plants, operating through a context-dependent dual function that activates and represses distinct subsets of meiotic genes to ensure their expression at the right time and place during reproductive development. Given that DREAM dysfunction causes reproductive defects across animals and that testis-specific DREAM variants have evolved in both mammals and *Drosophila* to fulfill activating roles in meiosis, the regulatory logic uncovered here is likely conserved across multicellular eukaryotes. Our identification of *MER3* as a direct target of DREAM complex components, whose function in meiocytes may involve a specialized complex variant, provides the first mechanistic understanding into how these components control the meiotic recombination program and provides additional insights into understanding how the composition and context specificity of DREAM complexes are tuned to meet the transcriptional requirements of reproductive development.

MATERIALS AND METHODS

Plant materials

The *Arabidopsis thaliana* accession Columbia (Col-0) was used as a WT reference throughout this study. All mutants and transgenic

Downloaded from https://www.science.org at Institute of Science & Technology Austria (ISTA) on November 17, 2026

lines used in this study were in the Col-0 background. The transferred DNA insertion lines *tcx5-1* (SALK_047165), *tcx6-1* (GK-453H07), *aly1-1* (SALK_073108), *aly2-2* (SALK_118765C), *aly3-4* (SALK_125138C), *lin37a-2* (SALK_057175), *lin37b-3* (SALK_103139C), *lin52b-1* (GK_854A11), *mer3-2* (SALK_091560), *spo11-1-3* (SALK_146172), *mus81-2* (SALK_107515), and *msh4-1* (SALK_136296) were isolated from GABI-KAT and SALK transferred DNA collections and described previously (*3*). The *lin52a-c1* mutant is generated via CRISPR-Cas9 and described in our previous study (*3*). The *myb3r1-1*, *myb3r4-1*, *myb3r3-1*, and *myb3r5-1* alleles, and the *myb3r1-1 myb3r4-1* and *myb3r1-1 myb3r3-1 myb3r5-1* higher-order mutant combinations were previously described by Kobayashi *et al.* (*9*). Transgenic lines harboring PRO_{RPS5A}*:TagRFP:TUB5* (*45*) and PRO_{ASY3}*:ASY3:RFP* (*52*) reporter constructs were crossed with EGFP-TCX5, EGFP-TCX6, and EGFP-ALY1 transgenic reporter lines generated in this study. All plants were grown in growth chambers with a 16-hour light/21°C and 8-hour/18°C dark cycle.

Plasmid construction and plant transformation

To generate PRO_{TCX5}*:EGFP:TCX5* and PRO_{TCX6}*:EGFP:TCX6* reporter constructs, genomic sequences of *TCX5* (5557 bp) and TCX6 (5157 bp) were amplified by polymerase chain reaction (PCR) and subsequently cloned into the *pENTR* vector via the SLiCE reaction. A Sma I restriction site was introduced right after the start codon by PCR. The resulting construct was linearized by Sma I restriction and ligated with *EGFP*. To generate the PRO_{ALY1}*:ALY1-EGFP* construct, the genomic sequence of the *ALY1* (9252 bp) sequence was amplified as two fragments by PCR and inserted into the *pENTR* vector via the SLiCE reaction. A Sma I restriction site was introduced right before the stop codon by PCR. The resulting construct was linearized by Sma I restriction and ligated with *EGFP*. These constructs were subsequently transferred into the binary expression vector pGWB501 (*53*) by the Gateway LR reaction.

To generate the RBR1-binding domain mutant versions of TCX5 and TCX6, the LxCxE motif was mutated to AxAxA by reamplifying *pDONR221-TCX5* or *pDONR221-TCX6* with primers carrying the respective substitutions. The subsequent steps of EGFP fusion and cloning into the binary expression vector were performed as described above for the respective WT reporter constructs.

To generate PRO_{DMC1}*:MER3:EGFP:*TER_{REC8}, the genomic sequences of *MER3* covering the coding sequence (6259 bp) and an *EGFP* fragment were amplified by PCR and incorporated by the SLiCE reaction into the *pENTR-*PRO_{DMC1}*:SmaI:*TER_{REC8} vector linearized by Sma I restriction. The resulting fusion construct was then transferred into the binary expression vector pGWB501 by the Gateway LR reaction. All primers used for cloning are listed in table S4. *A. thaliana* transgenic lines were generated by *Agrobacterium*-mediated transformation (*54*).

Pollen and seed viability assessment

Pollen viability was assessed as previously described (*55*). Three open flowers per plant were dipped into 12 µl of Peterson staining solution (10% ethanol, 0.001% malachite green, 25% glycerol, 0.005% acid fuchsin, 0.0005% orange G, and 4% acetic acid). Slides were covered with a coverslip, incubated on a preheated hot plate at 80°C for 5 min, and screened using a light microscope (Axioskop, Carl Zeiss GmbH, Oberkochen, Germany) and the 20× objective. Six hundred pollen grains of five different plants were counted per line. To assess seed viability, seeds were evaluated from five siliques of at least five different plants per line.

Cell spreads

Flower buds from transgenic lines were fixed as previously described (*56*). Briefly, fresh flower buds were fixed in ethanol/acetic acid (3:1) for 48 hours at 4°C, washed with 75% ethanol three times, and stored in 70% ethanol at 4°C. For male meiotic spreads, flower buds between 0.3 and 0.5 mm in size were digested in an enzyme solution (10 mM citrate buffer containing 1.5% cellulose, 1.5% pectolyase, and 1.5% cytohelicase) for 3 hours at 37°C. Three digested flower buds were transferred onto a glass slide and mashed with a bent needle. The cell suspension was spread on an adhesive slide on a 46°C hot plate after adding 10 µl of 45% acetic acid. The slide was then rinsed with an ice-cold ethanol/acetic acid (3:1) solution and mounted in 15 µl of VECTASHIELD medium with DAPI (Vector Laboratories).

For female meiocyte spreads, fixed flowers were washed twice with distilled water. Carpels were isolated, washed once with the citrate buffer, and transferred onto a sealing film. Fifteen to 20 µl of enzyme solution was added, and samples were covered to prevent evaporation and incubated at 37°C for 1.5 hours. After enzymatic digestion, samples were washed once with distilled water, transferred onto glass slides, and gently squashed in a small drop of distilled water. Slides were treated with precooled 60% acetic acid, gently mixed, incubated on a 45°C hot plate for 1 to 2 min, and then immediately fixed with precooled Carnoy's solution (60% ethanol, 30% chloroform, and 10% glacial acetic acid). After air drying for 10 min, slides were stained with DAPI. Slides were observed using an Axiophot microscope (Zeiss) with a 63× oil-immersion objective.

DAPI staining of whole ovaries

To assess female meiotic progression, fixed flowers were washed twice with distilled water. The outer tissue of the carpel was carefully removed using fine forceps to expose the ovules. A drop of DAPI solution was applied to the ovules, which were subsequently covered with a coverslip and observed using a fluorescence microscope.

Immunostaining

Immunostaining was performed as previously described (*57*). Briefly, flower buds were dissected using needles, and anthers were transferred to a droplet of artificial pond water (0.5 mM NaCl, 0.4 mM $CaCl_2$, 0.2 mM $NaHCO_3$, and 0.05 mM KCl in deionized water) on a polylysine-coated slide. Anthers were gently squeezed to release meiocytes. The isolated meiocytes were collected into a 1.5-ml tube on ice and subsequently digested in 15 µl of digestion solution (1% cytohelicase, 1.5% sucrose, and 1% polyvinylpyrrolidone) in the dark for 30 min. Following digestion, meiocytes were transferred to a clean, charged microscope slide. Next, 20 µl of 1% Lipsol was added, and the sample was spread by tilting the slide. After a 4-min incubation at room temperature, 24 µl of 4% formaldehyde was added, and the slide was left to air dry. The slides were washed twice with 2× SCC (0.3 M NaCl and 30 mM $Na_3C_6H_5O_7$) for 5 min each. The primary antibody mix was then added, and the slide was covered by a piece of parafilm. Slides were incubated overnight at 4°C in a humid chamber. Slides were washed twice with 2× SCC for 5 min, followed by addition of the secondary antibody mix. Slides were again covered with parafilm and incubated for 1 hour at 37°C in a humid chamber. Last, slides were washed twice with 2× SCC for 5 min in the dark. Fifteen microliters of VECTASHIELD medium with DAPI was added to the slide and covered with a glass coverslip and sealed using nail polish. The following dilutions were used for the primary and secondary antibodies: anti-ASY1 1:10,000 (*57*), anti-RAD51 1:300

Downloaded from https://www.science.org at Institute of Science & Technology Austria (ISTA) on November 17, 2026

(*58*), anti-ZYP1 1:500 (*29*), anti-HEI10 1:300 (*57*), anti-guinea pig Alexa 488 1:400 (Abcam, no. ab150185), anti-rabbit Alexa 568 1:400 (Abcam, no. ab175471), and anti-rat Alexa 647 (Abcam, no. ab150159).

Microscopy

To detect protein localization in reporter lines, young anthers were dissected from floral buds in a drop of artificial pond water and imaged directly using an upright Zeiss LSM900 confocal microscope equipped with a 60× water-immersion objective. Meiotic stages were determined on the basis of chromosome morphology, cell shape, or microtubule pattern visualized by the *PRO$_{RPS5A}$:TagRFP:TUA5* marker. Green fluorescent protein (GFP) was excited at 488 nm and detected at 495 to 560 nm, and TagRFP was excited at 561 nm and detected at 570 to 650 nm.

For imaging immunohistochemical stained samples, high-resolution imaging was performed using a Zeiss LSM 880 confocal microscope equipped with an Airyscan detector (Zeiss, Oberkochen, Germany), using a 63×/1.4–numerical aperture oil-immersion objective. Airyscan mode was used to improve the resolution and signal-to-noise ratio. Z-stacks were acquired at optimal intervals for three-dimensional reconstruction and processed using Zeiss Zen Black software (ZEN 2.3 SP1).

Male meiocyte isolation and RNA extraction

Anthers at developmental stages 6 to 11 covering all meiotic stages were dissected and collected in artificial pond water supplemented with RNasin Ribonuclease Inhibitor (1 U/μl; Promega, N2511). Anthers were gently squashed to release meiotic columns, and ~300 columns per sample were transferred into ZR BashingBead Lysis Tubes (Zymo Research, S6003-50) containing lysis buffer from the RNAqueous-Micro Total RNA Isolation Kit (Thermo Fisher Scientific, AM1931) and then immediately flash-frozen in liquid nitrogen. Dissections and collections were performed at 4°C from 16 plants per genotype for each replicate across three biological replicates. Samples were homogenized using a mechanical shaker, and total RNA was extracted according to the manufacturer's protocol. RNA quality was assessed using an Agilent 2100 Bioanalyzer with the NanoChip Kit, and all samples showed high integrity (RNA integrity number >8.0).

Transcriptome sequencing and data analysis

RNA sequencing libraries were prepared by Novogene and sequenced on an Illumina HiSeq X Ten platform using 150-bp paired-end reads (PE150). Raw read quality was assessed using FastQC. The reference genome index was built with HISAT2 (version 2.0.5), and paired-end reads were aligned to the genome using the same version. Gene-level read counts were obtained using featureCounts (version 1.5.0-p3). Transcript assembly and quantification were performed with StringTie (version 1.3.3b), and gene expression levels were reported as fragments per kilobase of exon per million fragments mapped (FPKM). Next, we used DESeq2 to identify DEGs with the thresholds: adjusted $P < 0.05$ and $|\log_2 \text{fold change}| > 0.5$. GO enrichment analysis of DEGs was performed using agriGO (*59*) version 2.0 (https://systemsbiology.cau.edu.cn/agriGOv2/). GO terms with an adjusted $P < 0.05$ were considered significantly enriched.

CUT&Tag sample preparation from *Arabidopsis* anthers

Anthers at stages 6 to 11 from the *PRO$_{TCX5}$:EGFP:TCX5 tcx5* transgenic line were dissected to capture all stages of meiosis and collected in Nuclei Extraction Buffer [0.25 M sucrose, 10 mM tris-HCl (pH 8.0), 10 mM $MgCl_2$, and 1% Triton X-100] supplemented with a protease inhibitor cocktail (cOmplete ULTRA Tablets, Roche, 05892791001). Anthers were homogenized using a glass Dounce tissue grinder and incubated on a rotating wheel at 4°C for 10 min. The homogenate was filtered through 50-μm filters, and nuclei were pelleted by centrifugation at 1000*g* for 10 min at 4°C. Nuclei were washed three times with the same extraction buffer. The final pellet was resuspended in sucrose buffer [0.25 M sucrose, 10 mM tris-HCl (pH 8.0), and 10 mM $MgCl_2$] containing a protease inhibitor cocktail (cOmplete ULTRA Tablets, Roche, 05892791001) and 10% dimethyl sulfoxide. Extracted nuclei were cryopreserved at −80°C in a controlled-rate freezing container. CUT&Tag was performed using the CUT&Tag-IT Assay Kit, Anti-Rabbit (Active Motif, 53160), with an anti-GFP antibody (Thermo Fisher Scientific, A-11122) used to target EGFP-tagged TCX5. Library preparation was carried out according to the manufacturer's protocol.

CUT&TAG data analysis

Paired-end reads of CUT&Tag raw data were trimmed by using Fastp (version 0.23.2). Using Bowtie2 (version 2.5.4) (*60*), the cleaned reads were aligned to the *Arabidopsis* reference genome assembly TAIR10. Duplicated reads were removed, and reads were filtered to keep only high-quality alignments (mapping quality score >30) using SAMtools (version 1.9) (*61*). Afterward, peaks were called using MACS3 (https://github.com/macs3-project/MACS) (*62*) with the threshold *q* value <0.05. ChIPseeker from the R package was used to investigate genomic distribution of CUT&Tag peaks. For genome-wide analyses, TCX5 targets were defined as regions with a fold enrichment >4. For analyses focusing on the promoters of the 135 meiotic genes (table S3), the fold-enrichment threshold was set to >2 to reduce the possibility of false negatives, given the low proportion of meiotic cells in anther tissues. To visualize the signals of CUT&Tag, RPGC-normalized bigWig files were generated using the bamCoverage option from Deeptools (version 3.5.6) (*63*). Motif enrichment analysis of TCX5 binding sites was conducted using findMotifsGenome.pl from HOMER, identifying motifs enriched with $P < 0.05$, which was determined by a binomial test.

Dual-luciferase reporter assay

To assess the transcriptional regulatory activity of TCX5 and TCX6 on the *MER3* promoter, different promoter fragments were individually cloned upstream of the firefly luciferase (LUC) reporter gene in the pGreenII 0800-LUC vector, which additionally carries a *Renilla* luciferase (REN) gene under the control of the cauliflower mosaic virus (CaMV) 35*S* promoter as an internal reference. TCX5 and TCX6 were used as effectors in transient coexpression assays carried out in *Nicotiana benthamiana* leaves via *Agrobacterium*-mediated infiltration. LUC and REN activities were subsequently measured using the Dual-Luciferase Reporter Assay System (Promega, E1910), and LUC signals were normalized to REN activity to account for variation in transformation efficiency. The assay was performed in three independent biological replicates. Primers used for amplification of the *MER3* promoter fragments are listed in table S4.

Image processing and HEI10 and RAD51 focus quantification

For image analysis of RAD51 and HEI10 immunostaining, maximum intensity projections were generated using the Z Project function in Fiji/ImageJ (version 2.14.0/1.54f). RAD51and HEI10 foci

Downloaded from https://www.science.org at Institute of Science & Technology Austria (ISTA) on November 17, 2026

were manually counted on merged channels. Only RAD51 and HEI10 foci colocalizing with the chromosome markers (ASY1 and ZYP1, respectively) were included in the analysis. To ensure consistency across samples, all images were adjusted with identical brightness and contrast settings.

Statistical analysis

All statistical analyses (as indicated in the figure legends) were performed using GraphPad Prism software (GraphPad Software version 10.4.1). Error bars indicate standard deviations.

Supplementary Materials

The PDF file includes:

Figs. S1 to S10
Tables S1, S2 and S4
Legend for table S3

Other Supplementary Material for this manuscript includes the following:

Table S3

REFERENCES

1. M. Fischer, G. A. Müller, Cell cycle transcription control: DREAM/MuvB and RB-E2F complexes. *Crit. Rev. Biochem. Mol. Biol.* **52**, 638–662 (2017).
2. M. Fischer, A. E. Schade, T. B. Branigan, G. A. Müller, J. A. DeCaprio, Coordinating gene expression during the cell cycle. *Trends Biochem. Sci.* **47**, 1009–1022 (2022).
3. L. Lang, A. Pettkó-Szandtner, H. Tunçay Elbaşı, H. Takatsuka, Y. Nomoto, A. Zaki, S. Dorokhov, G. De Jaeger, D. Eeckhout, M. Ito, Z. Magyar, L. Bögre, M. Heese, A. Schnittger, The DREAM complex represses growth in response to DNA damage in *Arabidopsis*. *Life Sci. Alliance* **4**, e202101141 (2021).
4. Y. Q. Ning, N. Liu, K. K. Lan, Y. N. Su, L. Li, S. Chen, X. J. He, DREAM complex suppresses DNA methylation maintenance genes and precludes DNA hypermethylation. *Nat. Plants* **6**, 942–956 (2020).
5. M. G. Koliopoulos, R. Muhammad, T. I. Roumeliotis, F. Beuron, J. S. Choudhary, C. Alfieri, Structure of a nucleosome-bound MuvB transcription factor complex reveals DNA remodelling. *Nat. Commun.* **13**, 5075 (2022).
6. S. Sadasivam, S. Duan, J. A. DeCaprio, The MuvB complex sequentially recruits B-Myb and FoxM1 to promote mitotic gene expression. *Genes Dev.* **26**, 474–489 (2012).
7. M. Fischer, P. Grossmann, M. Padi, J. A. DeCaprio, Integration of TP53, DREAM, MMB-FOXM1 and RB-E2F target gene analyses identifies cell cycle gene regulatory networks. *Nucleic Acids Res.* **44**, 6070–6086 (2016).
8. D. Georlette, S. Ahn, D. M. MacAlpine, E. Cheung, P. W. Lewis, E. L. Beall, S. P. Bell, T. Speed, J. R. Manak, M. R. Botchan, Genomic profiling and expression studies reveal both positive and negative activities for the *Drosophila* Myb–MuvB/dREAM complex in proliferating cells. *Genes Dev.* **21**, 2880–2896 (2007).
9. K. Kobayashi, T. Suzuki, E. Iwata, N. Nakamichi, T. Suzuki, P. Chen, M. Ohtani, T. Ishida, H. Hosoya, S. Müller, T. Leviczky, A. Pettkó-Szandtner, Z. Darula, A. Iwamoto, M. Nomoto, Y. Tada, T. Higashiyama, T. Demura, J. H. Doonan, M. Hauser, K. Sugimoto, M. Umeda, Z. Magyar, L. Bögre, M. Ito, Transcriptional repression by MYB3R proteins regulates plant organ growth. *EMBO J.* **34**, 1992–2007 (2015).
10. Y. Wang, Y. Fan, D. Fan, Y. Zhang, X. Zhou, R. Zhang, Y. Wang, Y. Sun, The *Arabidopsis* DREAM complex antagonizes WDR5A to modulate histone H3K4me2/3 deposition for a subset of genome repression. *Proc. Natl. Acad. Sci. U.S.A.* **119**, e2206075119 (2022).
11. L. Lang, F. Böwer, H. T. Elbaşı, D. Eeckhout, N. Marschlich, G. de Jaeger, M. Heese, A. Schnittger, The two plant-specific DREAM components FLIC and FLAC repress floral transition in *Arabidopsis*. bioRxiv 2023.08.07.552284 [Preprint] (2023). https://doi.org/10.1101/2023.08.07.552284.
12. T. M. Tabuchi, B. Deplancke, N. Osato, L. J. Zhu, M. I. Barrasa, M. M. Harrison, H. R. Horvitz, A. J. M. Walhout, K. A. Hagstrom, Chromosome-biased binding and gene regulation by the *Caenorhabditis elegans* DRM complex. *PLOS Genet.* **7**, e1002074 (2011).
13. J. Jiang, E. Benson, N. Bausek, K. Doggett, H. White-Cooper, Tombola, a tesmin/TSO1-family protein, regulates transcriptional activation in the *Drosophila* male germline and physically interacts with always early. *Development* **134**, 1549–1559 (2007).
14. A. Oji, A. Isotani, Y. Fujihara, J. M. Castaneda, S. Oura, M. Ikawa, TESMIN, METALLOTHIONEIN-LIKE 5, is required for spermatogenesis in mice. *Biol. Reprod.* **102**, 975–983 (2020).
15. X. Zhang, M. Li, X. Jiang, H. Ma, S. Fan, Y. Li, C. Yu, J. Xu, R. Khan, H. Jiang, Q. Shi, Nuclear translocation of MTL5 from cytoplasm requires its direct interaction with LIN9 and is essential for male meiosis and fertility. *PLOS Genet.* **17**, e1009753 (2021).
16. S. Keeney, C. N. Giroux, N. Kleckner, Meiosis-specific DNA double-strand breaks are catalyzed by Spo11, a member of a widely conserved protein family. *Cell* **88**, 375–384 (1997).
17. M. Grelon, D. Vezon, G. Gendrot, G. Pelletier, AtSPO11-1 is necessary for efficient meiotic recombination in plants. *EMBO J.* **20**, 589–600 (2001).
18. S. J. Armstrong, A. P. Caryl, G. H. Jones, F. C. H. Franklin, Asy1, a protein required for meiotic chromosome synapsis, localizes to axis-associated chromatin in *Arabidopsis* and *Brassica*. *J. Cell Sci.* **115**, 3645–3655 (2002).
19. M. Ferdous, J. D. Higgins, K. Osman, C. Lambing, E. Roitinger, K. Mechtler, S. J. Armstrong, R. Perry, M. Pradillo, N. Cuñado, F. C. H. Franklin, Inter-homolog crossing-over and synapsis in *Arabidopsis* meiosis are dependent on the chromosome axis protein AtASY3. *PLOS Genet.* **8**, e1002507 (2012).
20. O. D. Ines, K. Abe, C. Goubely, M. E. Gallego, C. I. White, Differing Requirements for RAD51 and DMC1 in meiotic pairing of centromeres and chromosome arms in *Arabidopsis thaliana*. *PLOS Genet.* **8**, e1002636 (2012).
21. V. Cloud, Y.-L. Chan, J. Grubb, B. Budke, D. K. Bishop, Rad51 is an accessory factor for Dmc1-mediated joint molecule formation during meiosis. *Science* **337**, 1222–1225 (2012).
22. D. Zickler, N. Kleckner, Recombination, pairing, and synapsis of homologs during meiosis. *Cold Spring Harb. Perspect. Biol.* **7**, a016626 (2015).
23. F. Baudat, B. de Massy, Regulating double-stranded DNA break repair towards crossover or non-crossover during mammalian meiosis. *Chromosome Res.* **15**, 565–577 (2007).
24. D. K. Bishop, D. Zickler, Early decision: Meiotic crossover interference prior to stable strand exchange and synapsis. *Cell* **117**, 9–15 (2004).
25. C. Chen, W. Zhang, L. Timofejeva, Y. Gerardin, H. Ma, The *Arabidopsis* ROCK-N-ROLLERS gene encodes a homolog of the yeast ATP-dependent DNA helicase MER3 and is required for normal meiotic crossover formation. *Plant J.* **43**, 321–334 (2005).
26. P. Lu, A. J. Wijeratne, Z. Wang, G. P. Copenhaver, H. Ma, *Arabidopsis* PTD is required for type I crossover formation and affects recombination frequency in two different chromosomal regions. *J. Genet. Genomics* **41**, 165–175 (2014).
27. N. Macaisne, J. Vignard, R. Mercier, SHOC1 and PTD form an XPF–ERCC1-like complex that is required for formation of class I crossovers. *J. Cell Sci.* **124**, 2687–2691 (2011).
28. L. Chelysheva, G. Gendrot, D. Vezon, M. P. Doutriaux, R. Mercier, M. Grelon, Zip4/Spo22 is required for class I CO formation but not for synapsis completion in *Arabidopsis thaliana*. *PLOS Genet.* **3**, 802–813 (2007).
29. J. D. Higgins, J. Vignard, R. Mercier, A. G. Pugh, F. C. H. Franklin, G. H. Jones, AtMSH5 partners AtMSH4 in the class I meiotic crossover pathway in *Arabidopsis thaliana*, but is not required for synapsis. *Plant J.* **55**, 28–39 (2008).
30. L. Chelysheva, D. Vezon, A. Chambon, G. Gendrot, L. Pereira, A. Lemhemdi, N. Vrielynck, S. Le Guin, M. Novatchkova, M. Grelon, The *Arabidopsis* HEI10 is a new ZMM protein related to Zip3. *PLOS Genet.* **8**, e1002799 (2012).
31. S. Sadasivam, J. A. DeCaprio, The DREAM complex: Master coordinator of cell cycle-dependent gene expression. *Nat. Rev. Cancer* **13**, 585–595 (2013).
32. W. Crismani, C. Girard, N. Froger, M. Pradillo, J. L. Santos, L. Chelysheva, G. P. Copenhaver, C. Horlow, R. Mercier, FANCM limits meiotic crossovers. *Science* **336**, 1588–1590 (2012).
33. J. D. Higgins, M. Ferdous, K. Osman, F. C. H. Franklin, The RecQ helicase AtRECQ4A is required to remove inter-chromosomal telomeric connections that arise during meiotic recombination in *Arabidopsis*. *Plant J.* **65**, 492–502 (2011).
34. M. Séguéla-Arnaud, W. Crismani, C. Larchevêque, J. Mazel, N. Froger, S. Choinard, A. Lemhemdi, N. Macaisne, J. Van Leene, K. Gevaert, G. De Jaeger, L. Chelysheva, R. Mercier, Multiple mechanisms limit meiotic crossovers: TOP3α and two BLM homologs antagonize crossovers in parallel to FANCM. *Proc. Natl. Acad. Sci. U.S.A.* **112**, 4713–4718 (2015).
35. H. Serra, C. Lambing, C. H. Griffin, S. D. Topp, M. Séguéla-Arnaud, J. Fernandes, R. Mercier, I. R. Henderson, Massive crossover elevation via combination of HEI10 and recq4a recq4b during *Arabidopsis* meiosis. bioRxiv 159764 [Preprint] (2017). https://doi.org/10.1101/159764.
36. R. Mercier, S. Jolivet, D. Vezon, E. Huppe, L. Chelysheva, M. Giovanni, F. Nogué, M.-P. Doutriaux, C. Horlow, M. Grelon, C. Mézard, Two meiotic crossover classes cohabit in *Arabidopsis*: One is dependent on MER3, whereas the other one is not. *Curr. Biol.* **15**, 692–701 (2005).
37. P. D. Goetsch, J. M. Garrigues, S. Strome, Loss of the *Caenorhabditis elegans* pocket protein LIN-35 reveals MuvB's innate function as the repressor of DREAM target genes. *PLOS Genet.* **13**, e1007088 (2017).
38. A. Bujarrabal-Dueso, G. Sendtner, D. H. Meyer, G. Chatzinikolaou, K. Stratigi, G. A. Garinis, B. Schumacher, The DREAM complex functions as conserved master regulator of somatic DNA-repair capacities. *Nat. Struct. Mol. Biol.* **30**, 475–488 (2023).
39. L. Abbasova, P. Urbanaviciute, D. Hu, J. N. Ismail, B. M. Schilder, A. Nott, N. G. Skene, S. J. Marzi, CUT&Tag recovers up to half of ENCODE ChIP-seq histone acetylation peaks. *Nat. Commun.* **16**, 2993 (2025).
40. Y. Guo, X. Zheng, T. Wang, X. He, J. Li, C. Wang, C. You, A. Schnittger, J. Qi, J. Wang, Y. Wang, Suppression of meiotic double strand break formation in somatic cells by TCX5/6 maintains genome stability. *Sci. Adv.* **12** , eaef7208 (2026).

Downloaded from https://www.science.org at Institute of Science & Technology Austria (ISTA) on November 17, 2026

41. J.-Y. Bleuyard, C. I. White, The *Arabidopsis* homologue of Xrcc3 plays an essential role in meiosis. *EMBO J.* **23**, 439–449 (2004).
42. M. Grelon, G. Gendrot, D. Vezon, G. Pelletier, The *Arabidopsis* MEI1 gene encodes a protein with five BRCT domains that is involved in meiosis-specific DNA repair events independent of SPO11-induced DSBs. *Plant J. Cell Mol. Biol.* **35**, 465–475 (2003).
43. I. d'Erfurth, S. Jolivet, N. Froger, O. Catrice, M. Novatchkova, M. Simon, E. Jenczewski, R. Mercier, Mutations in AtPS1 (*Arabidopsis thaliana* Parallel Spindle 1) lead to the production of diploid pollen grains. *PLOS Genet.* **4**, e1000274 (2008).
44. P. P. Laktionov, D. A. Maksimov, S. E. Romanov, P. A. Antoshina, O. V. Posukh, H. White-Cooper, D. E. Koryakov, S. N. Belyakin, Genome-wide analysis of gene regulation mechanisms during *Drosophila* spermatogenesis. *Epigenetics Chromatin* **11**, 14 (2018).
45. T. M. Tabuchi, A. Rechtsteiner, S. Strome, K. A. Hagstrom, Opposing activities of DRM and MES-4 tune gene expression and X-chromosome repression in *Caenorhabditis elegans* germ cells. *G3 GenesGenomesGenetics* **4**, 143–153 (2014).
46. S. Oura, A. Ninomiya, F. Sugihara, M. M. Matzuk, M. Ikawa, Proximity-dependent biotin labeling in testicular germ cells identified TESMIN-associated proteins. *Sci. Rep.* **12**, 22198 (2022).
47. E. Bolcun-Filas, L. A. Bannister, A. Barash, K. J. Schimenti, S. A. Hartford, J. J. Eppig, M. A. Handel, L. Shen, J. C. Schimenti, A-MYB (MYBL1) transcription factor is a master regulator of male meiosis. *Development* **138**, 3319–3330 (2011).
48. E. L. Beall, P. W. Lewis, M. Bell, M. Rocha, D. L. Jones, M. R. Botchan, Discovery of tMAC: A *Drosophila* testis-specific meiotic arrest complex paralogous to Myb-Muv B. *Genes Dev.* **21**, 904–919 (2007).
49. J. Jiang, H. White-Cooper, Transcriptional activation in *Drosophila* spermatogenesis involves the mutually dependent function of aly and a novel meiotic arrest gene cookie monster. *Development* **130**, 563–573 (2003).
50. K. Doggett, J. Jiang, G. Aleti, H. White-Cooper, Wake-up-call, a lin-52 paralogue, and Always early, a lin-9 homologue physically interact, but have opposing functions in regulating testis-specific gene expression. *Dev. Biol.* **355**, 381–393 (2011).
51. P. Laktionov, H. White-Cooper, D. Maksimov, S. Belyakin, Transcription factor Comr acts as a direct activator in the genetic program controlling spermatogenesis in *D. melanogaster*. *Mol. Biol.* **48**, 130–140 (2014).
52. M. Balboni, C. Yang, S. Komaki, J. Brun, A. Schnittger, COMET functions as a PCH2 cofactor in regulating the horma domain protein ASY1. *Curr. Biol.* **30**, 4113–4127.e6 (2020).
53. T. Nakagawa, T. Suzuki, S. Murata, S. Nakamura, T. Hino, K. Maeo, R. Tabata, T. Kawai, K. Tanaka, Y. Niwa, Y. Watanabe, K. Nakamura, T. Kimura, S. Ishiguro, Improved gateway binary vectors: High-performance vectors for creation of fusion constructs in transgenic analysis of plants. *Biosci. Biotechnol. Biochem.* **71**, 2095–2100 (2007).
54. X. Zhang, R. Henriques, S.-S. Lin, Q.-W. Niu, N.-H. Chua, *Agrobacterium*-mediated transformation of *Arabidopsis thaliana* using the floral dip method. *Nat. Protoc.* **1**, 641–646 (2006).
55. R. Peterson, J. P. Slovin, C. Chen, A simplified method for differential staining of aborted and non-aborted pollen grains. *Int. J. Plant Biol.* **1**, e13 (2010).
56. C. Yang, K. Sofroni, E. Wijnker, Y. Hamamura, L. Carstens, H. Harashima, S. C. Stolze, D. Vezon, L. Chelysheva, Z. Orban-Nemeth, G. Pochon, H. Nakagami, P. Schlögelhofer, M. Grelon, A. Schnittger, The *Arabidopsis* Cdk1/Cdk2 homolog CDKA ;1 controls chromosome axis assembly during plant meiosis. *EMBO J.* **39**, e101625 (2019).
57. J. Sims, P. Schlögelhofer, M. T. Kurzbauer, From microscopy to nanoscopy: Defining an *Arabidopsis thaliana* meiotic atlas at the nanometer scale. *Front. Plant Sci.* **12**, 672914 (2021).
58. M.-T. Kurzbauer, C. Uanschou, D. Chen, P. Schlögelhofer, The recombinases DMC1 and RAD51 are functionally and spatially separated during meiosis in *Arabidopsis*. *Plant Cell* **24**, 2058–2070 (2012).
59. T. Tian, Y. Liu, H. Yan, Q. You, X. Yi, Z. Du, W. Xu, Z. Su, agriGO v2.0: A GO analysis toolkit for the agricultural community, 2017 update. *Nucleic Acids Res.* **45**, W122–W129 (2017).
60. B. Langmead, S. L. Salzberg, Fast gapped-read alignment with Bowtie 2. *Nat. Methods* **9**, 357–359 (2012).
61. H. Li, B. Handsaker, A. Wysoker, T. Fennell, J. Ruan, N. Homer, G. Marth, G. Abecasis, R. Durbin, 1000 Genome Project Data Processing Subgroup, The Sequence Alignment/Map format and SAMtools. *Bioinformatics* **25**, 2078–2079 (2009).
62. Y. Zhang, T. Liu, C. A. Meyer, J. Eeckhoute, D. S. Johnson, B. E. Bernstein, C. Nusbaum, R. M. Myers, M. Brown, W. Li, X. S. Liu, Model-based analysis of ChIP-Seq (MACS). *Genome Biol.* **9**, R137 (2008).
63. F. Ramírez, F. Dündar, S. Diehl, B. A. Grüning, T. Manke, deepTools: A flexible platform for exploring deep-sequencing data. *Nucleic Acids Res.* **42**, W187–W191 (2014).

Acknowledgments: We thank M. Heese for critical reading of the manuscript. We thank M. Köhler and R. B. Chaouche for valuable contribution to this work. We thank M. Ito for providing the *myb3r* mutant lines. We thank S. Uno for providing the *pENTR-PRO$_{DMC1}$:SmaI:TER$_{REC8}$* construct. **Funding:** This work was supported by the following: European Union and the Free and Hanseatic City of Hamburg Pro-Exzellenzia Plus fellowship (HT), Deutsche Forschungsgemeinschaft (DFG) grant SCHN 736/16-1 (to A.S.), National Natural Science Foundation of China (grant U24A20350), Guangdong S&T Program (2025B0202050002), and the Guangdong Ninth Pearl River Talent Program "Team of plant meiosis recombination and germplasm innovation" (2021ZT09N333).
Author contributions: Conceptualization: H.T., M.B., and A.S. Data curation: X.M., and Y.G. Formal analysis: H.T., X.M., F.B., M.B., and A.S. Funding acquisition: H.T., Y.W., M.B., and A.S. Investigation: H.T., X.M., K.M., H.F., V.F.T., L.L., D.L., and M.B. Methodology: H.T., M.B., and A.S. Project administration: M.B. and A.S. Resources: H.T., D.L., and A.S. Software: X.M. Supervision: Y.W., M.B., and A.S. Validation: H.T. Visualization: H.T., X.M., and M.B. Writing—original draft: H.T. and A.S. Writing—review and editing: H.T., M.B., and A.S. **Competing interests:** The authors declare that they have no competing interests. **Data, code, and materials availability:** All data and code needed to evaluate and reproduce the results in the paper are present in the paper and/or the Supplementary Materials. No custom code was generated for this study; all analyses used publicly available software as cited in Materials and Methods. The RNA-seq and CUT&Tag data generated in this study have been deposited in the Gene Expression Omnibus (GEO) under accession numbers GSE302287 (www.ncbi.nlm.nih.gov/geo/query/acc.cgi?acc=GSE302287) and GSE302286 (www.ncbi.nlm.nih.gov/geo/query/acc.cgi?acc=GSE302286), respectively. Materials generated in this study include double-mutant combinations of core DREAM components [with the exception of *lin37a/b*, which was generated in a previous study (*3*)]; the *PRO$_{TCX5}$:EGFP:TCX5*, *PRO$_{TCX6}$:EGFP:TCX6*, and *PRO$_{ALY1}$:ALY1-EGFP* genomic reporter constructs, RBR1-binding-domain mutant versions of the *TCX5* and *TCX6* constructs and their corresponding transgenic reporter lines; the *PRO$_{DMC1}$:MER3:EGFP:TER$_{REC8}$* construct and transgenic lines carrying this construct in the *mer3*, *aly1/2*, and *tcx5/6* backgrounds; and the *MER3* promoter constructs used for the luciferase reporter assay. All materials newly generated in this study are available from the corresponding author A.S. (arp.schnittger@uni-hamburg.de) upon request.

Submitted 7 January 2026
Accepted 14 September 2026
Published 16 October 2026
10.1126/sciadv.aef2922

Downloaded from https://www.science.org at Institute of Science & Technology Austria (ISTA) on November 17, 2026

ScienceAdvances

Transcriptional control of meiotic recombination by DREAM complex components

Hasibe Tunçay, Xing Ma, Katja Müller, Yuxuan Guo, Valerio Filippo Toccaceli, Huiqi Fu, Franziska Böwer, Lucas Lang, David Latrasse, Yingxiang Wang, Moussa Benhamed, and Arp Schnittger

Sci. Adv. **12** (42), eaef2922. DOI: 10.1126/sciadv.aef2922

View the article online
https://www.science.org/doi/10.1126/sciadv.aef2922
Permissions
https://www.science.org/help/reprints-and-permissions

Downloaded from https://www.science.org at Institute of Science & Technology Austria (ISTA) on November 17, 2026

Use of this article is subject to the Terms of service

Science Advances (ISSN 2375-2548) is published by the American Association for the Advancement of Science. 1200 New York Avenue NW, Washington, DC 20005. The title *Science Advances* is a registered trademark of AAAS.

Copyright © 2026 The Authors, some rights reserved; exclusive licensee American Association for the Advancement of Science. No claim to original U.S. Government Works. Distributed under a Creative Commons Attribution NonCommercial License 4.0 (CC BY-NC).